

EFFECT OF THERMOMECHANICAL TREATMENT ON STRUCTURAL PHENOMENA AND ELECTROCONDUCTIVITY IN COPPER CONDUCTORS

¹Lenka KUNČICKÁ, ²Petr KAČOR, ¹Jiří DVOŘÁK, ¹Zdeněk JAKUBEK

¹*Institute of Physics of Materials, Czech Academy of Sciences, Brno, Czech Republic, EU,*
kuncicka@ipm.cz, dvorak@ipm.cz, jakubek@ipm.cz

²*Department of Electrical Power Engineering, VŠB–TU Ostrava, Ostrava-Poruba, Czech Republic, EU,*
petr.kacor@vsb.cz

<https://doi.org/10.37904/metal.2022.4399>

Abstract

Despite its relatively high cost, copper is still the most popular electroconductive material. Its electroconductivity can be affected via structure modifications introduced by shear mixing, i.e. deformation processing, and/or thermomechanical treatment. Being an industrially applicable method of intensive plastic deformation, advantageously used to impart shear mixing, rotary swaging is favourable for production of long electroconductive wires. This study is focused on assessment of the effects of thermomechanical treatment on structural phenomena within copper conductors; the treatment consisted of room temperature rotary swaging and subsequent annealing. The results showed that the deformation ratio introduced via swaging was sufficient to impart homogenization of structure as the differences between the grain sizes and texture orientations within the peripheral and axial regions of the conductor were minimal. On the other hand, the swaged and annealed conductor featured slight inhomogeneity between the peripheral and axial regions, especially as regards structure regeneration and the occurrence of twinning, which was more pronounced in the axial region of the thermomechanically processed conductor (the volume fraction of <111> 60° twin boundaries was 60 % within this sample region). Interestingly, the electroconductivity was higher than 100 % IACS (International Annealed Copper Standard) for the swaged conductor, and even increased up to 104.4 % IACS for the annealed conductor due to the structure modifications imparted by the applied heat treatment.

Keywords: Copper, electroconductivity, rotary swaging, thermomechanical processing

1. INTRODUCTION

Copper and Cu-based alloys and composites are popular and widely used electroconductive materials [1,2]. However, high electric conductivity and high strength are mutually exclusive. Pure Cu features high electric conductivity, but exhibits very low mechanical strength (yield strength of 10–20 MPa, depending on purity) [3]. Among the solutions to improve mechanical properties of Cu is adding alloying elements, which provide increase in strength [4]. Nevertheless, alloying elements generally deteriorate electric conductivity due to electrons scattering [5]. Among the possibilities how to enhance the overall performance of Cu conductors and avoid alloying is the application of optimized deformation and/or thermomechanical treatment [6,7].

Thermomechanical treatment can advantageously be performed by methods of intensive and severe plastic deformation (SPD). Among the greatest advantages of these methods is that they impart shear mixing via imposing shear strain and thus promote generation of dislocations, formation of substructure, polygonization, and subsequent grain refinement, all of which introduce changes in mechanical, electrical, and utility properties [8,9]. SPD methods, such as HPT (high pressure torsion) [10], ECAP (equal channel angular pressing) [11]

and related methods – TCAP (twist channel angular pressing) [12], TCMAP (twist channel multi angular pressing) [13], ECAP-Conform [14], etc. – TE (twist extrusion) [15], FSP (friction stir processing) [16], ARB (accumulative roll bonding) [17] and others, are favourable to introduce significant substructure development and grain refinement. However, they are mostly discontinuous and thus limited to finite volumes of bulk samples. Therefore, SPD methods are generally not suitable to produce long wires (except a few, e.g. ECAP-Conform). On the other hand, the intensive plastic deformation method of rotary swaging is favourable for production of long axi-symmetrical products, including wires and conductors [18].

The presented study focused on assessment of the effects of rotary swaging and subsequent heat treatment on copper conductors swaged to the final diameter of 15 mm. We primarily focused on correlating the microstructure, i.e. grain sizes and orientations, as well as the occurrence of twins, with electric conductivity, which we characterized via IACS (International Annealed Copper Standard) values.

2. EXPERIMENT

Billets with the original diameter of 50 mm were made of electro-conductive CP (commercially pure) copper with the impurities of 0.015 wt.% P, 0.002 wt.% Zn, and 0.002 wt.% O. The billets were gradually rotary swaged at room temperature to conductors with the final diameter of 15 mm. One of the billets was subsequently subjected to heat treatment at 300 °C for 15 min. Within this study, the swaged conductor is denoted as *D15*, while the swaged and heat treated one is denoted as *D15TZ*. Structure analyses from the swaged (and heat treated) conductors were performed via scanning electron microscopy (Tescan Lyra 3 XMU FEG/SEMx/FIB microscope), particularly we used electron backscatter diffraction (EBSD) analyses (Symmetry EBSD detector). Preparation of samples involved transversal cutting of the conductors, and subsequent manual grinding, polishing and final electrolytic polishing of the cut samples. EBSD scans from 70° tilted samples were acquired with the scanning step of 0.1 μm. The results were evaluated using AZtecCrystal software. The analyses of grains and boundaries were performed with the limits of 5° for LAGBs (low angle grain boundaries), and 15° for HAGBs (high angle grain boundaries). The textures were evaluated with the deviation of 15°.

Electric resistivity of the rotary swaged Cu conductors was measured using the Four-Wire Resistance Measurements method. The measurement used two pairs of electrodes – sense and source probes – which were attached to the measured electro-conductive rod. The sense probes primarily served for *V1* voltage drop measurement, whereas the source probes served to supply the electric current. They could also be used to determine *V2* voltage drop via the constant $K = 0.0004 \Omega$; *I1* electric current could be characterized as equation (1).

$$I_1 = \frac{V_2}{K} \quad (1)$$

The values of *I1* and *V1* were subsequently used to calculate *R* electric resistivity of Cu conductor on measured length $L = 500$ mm via the Ohm's law (equation (2)).

$$R = \frac{V_1}{I_1} \quad (2)$$

Both the *V1* and *V2* voltage drop values were recorded during the experiment using a 24 bit resolution Data Acquisition card of NI-9238 type with the minimum sensitivity $dU = 60$ nV. The acquired data finally served to calculate ρ specific electric resistivity via equation (3).

$$\rho = R \cdot \frac{S}{L} = \frac{V_1}{I_1} \cdot \frac{S}{L} = \frac{V_1}{I_1} \cdot C \quad (3)$$

where *S* is area of cross-section of the conductor (m²), and *C* is constant of characteristic dimension (m).

3. RESULTS AND DISCUSSION

3.1. Microstructure

Orientation image map (OIM) of the original CP Cu with grain boundaries is shown in **Figure 1a**. As can be seen, the original Cu featured the majority of HAGBs and a high fraction of twins – almost 63% of $\langle 111 \rangle 60^\circ$ twin boundaries. Also, the average grain size was quite large – avg. maximum ferret diameter of 39.0 μm (the average grain sizes, together with standard deviations, are summarized in **Table 1**). The orientations of grains, i.e. texture, within the CP Cu was quite random, too, as evident from Inverse Pole Figures (IPFs) depicted in **Figure 1b**. The acquired findings were typical for a commercially available annealed Cu.

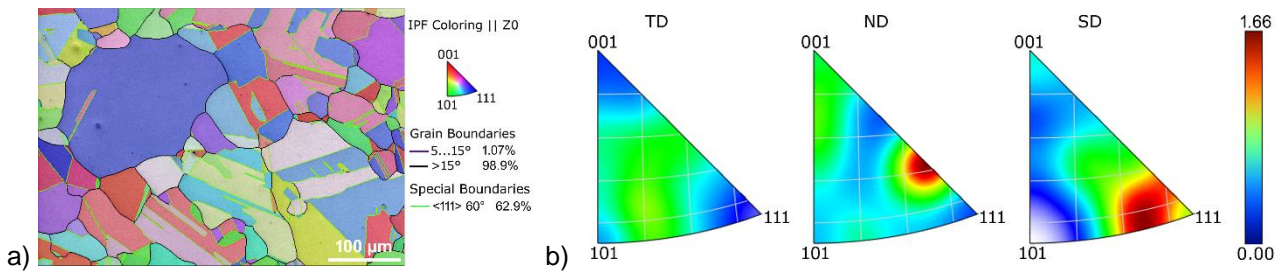


Figure 1 OIM showing microstructure of original CP Cu (a), IPF showing texture of original CP Cu (b)

Table 1 Summary of grain sizes for CP Cu, and *D15* and *D15TZ* conductors (two examined locations)

sample/location	CP Cu	D15/peripheral	D15/axial	D15TZ/peripheral	D15TZ/axial
grain size via max. ferret diameter (μm)	39.0	5.0	6.2	8.2	7.6
standard deviation (-)	36.3	7.4	8.0	9.6	7.3

OIM with highlighted grain boundaries for the peripheral region of the *D15* conductor is shown in **Figure 2a**, while the results of texture analyses represented by IPFs are depicted in **Figure 2b**. OIM with grain boundaries and IPFs for the axial region of the *D15* conductor are then depicted in **Figures 3a** and **3b**.

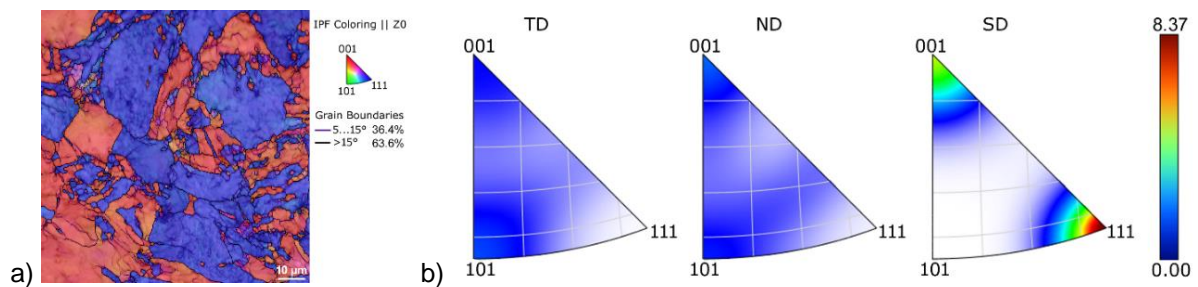


Figure 2 OIM acquired from periphery of *D15* conductor (a), IPFs from periphery of *D15* conductor (b)

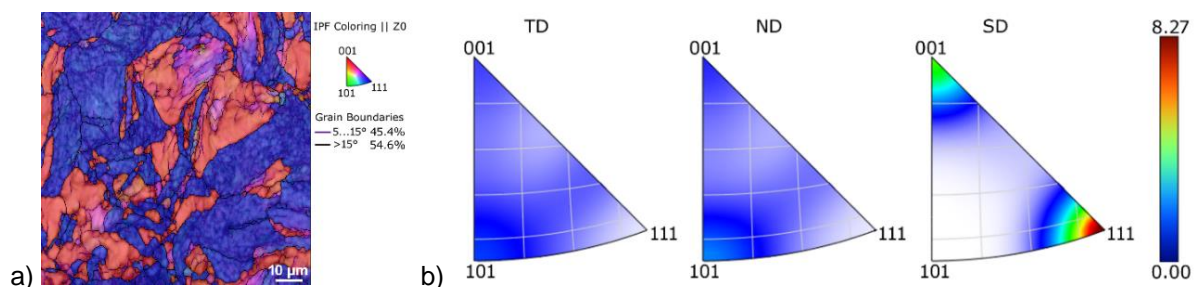


Figure 3 OIM acquired from axial region of *D15* conductor (a), IPFs from *D15* conductor axial region (b)

The results document that the room temperature swaging imparted grain refinement and formation of texture. The average grain size was 5.0 μm for the peripheral and 6.2 μm for the axial region of the *D15* conductor (**Table 1**). This difference can be attributed to the nature of the rotary swaging process, as the shear strain during swaging is imparted from the periphery towards the axis of a swaged semi-product [19]. This hypothesis was also supported by the fact that the grain size standard deviation was lower in the peripheral region of the *D15* conductor (see **Table 1**), and by the HAGBs analyses. Although the structures of both the *D15* conductor regions contained high fractions of HAGBs, the HAGBs fraction was higher at the periphery (compare 63.6% to 54.6% of HAGBs observed in the axial region), which points to significant development of dynamic restoration promoted by the effect of the intensive shear strain. Nevertheless, the orientation of the grains in both the regions was uniform; OIMs in **Figures 2a** and **3a** both show the dominance of $\langle 111 \rangle \parallel \text{SD}$ (swaging direction) and $\langle 001 \rangle \parallel \text{SD}$ orientations. These findings were confirmed by texture analyses – IPFs in **Figures 2b** and **3b** confirmed the presence of the mentioned texture fibres in comparable maximum intensities. Neither of the examined *D15* conductor regions exhibited any noticeable presence of twin boundaries.

The results of structure analyses of the *D15TZ* conductor peripheral region are depicted in **Figure 4a** (OIM with grain boundaries), and **Figure 4b** (IPFs), whereas OIM with grain boundaries and IPFs for the axial region of the *D15TZ* conductor are depicted in **Figures 5a** and **5b**, respectively. The applied heat treatment introduced increase in the average grain size – this value was 8.2 μm for the peripheral and 7.6 μm for the axial region of the *D15TZ* sample (**Table 1**). Interestingly, the grain size standard deviation was lower in the axial region of the *D15TZ* conductor than at its periphery. These phenomena can be explained by the mutual effect of the imposed shear strain and energy imparted by the applied heat treatment [20]. The fact that the grain size primarily increased at the periphery can be attributed to the amount of shear strain imposed during swaging, which was higher in this region and thus, in combination with the energy imparted by annealing, the final driving force for recrystallization and grain growth was higher at the periphery, which resulted in greater increase in the grain size. On the other hand, the imposed shear strain in the axial region was lower, which, in combination with the energy imparted by the heat treatment, resulted in structure, i.e. grain size, homogenization. These hypotheses were supported by the structure observations documented by **Figures 4a** and **5a**.

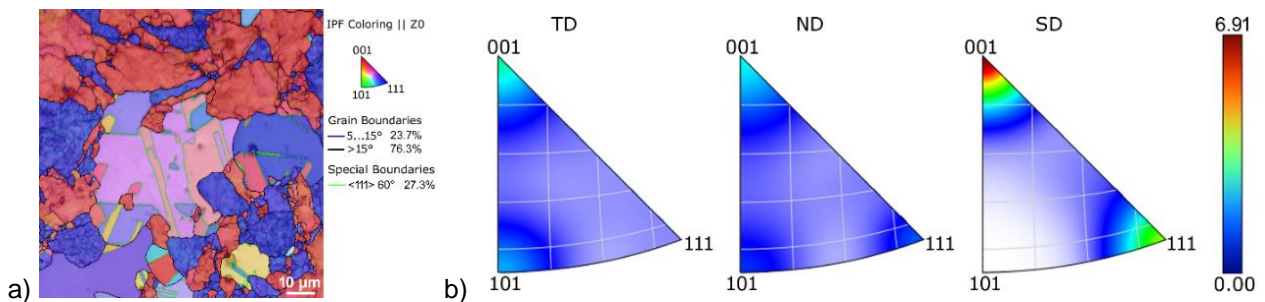


Figure 4 OIM acquired from periphery of *D15TZ* conductor (a), IPFs from periphery of *D15TZ* conductor (b)

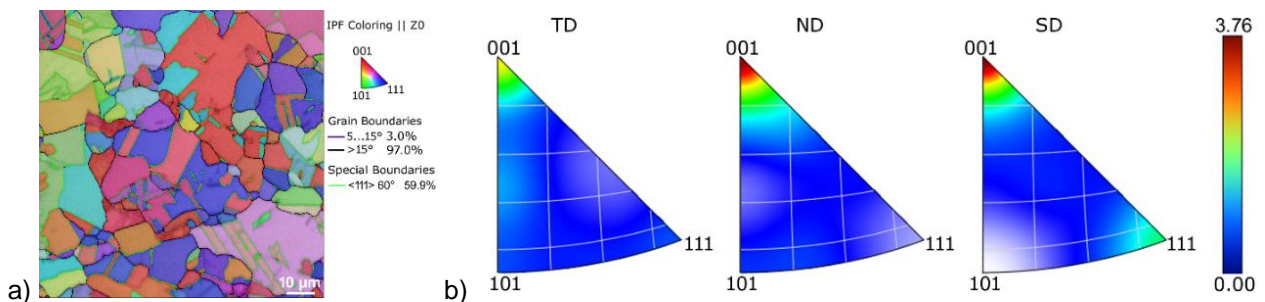


Figure 5 OIM from axial region of *D15TZ* conductor (a), IPFs from *D15TZ* conductor axial region (b)

The major effect of the heat treatment was on the grains morphology and their orientations. **Figures 4a** and **5a** show that the volume fractions of twins increased rapidly after the heat treatment – the fraction of the $\langle 111 \rangle 60^\circ$ twin boundaries was 27.3% in the axial region, and increased to 59.9% in the *D15TZ* peripheral region. The fraction of HAGBs increased significantly, too (up to 97% for the axial region), which points to the development of almost perfect recrystallization during annealing. The orientations of grains within both the regions also changed after the heat treatment, i.e. randomized (documented by **Figures 4b** and **5b**). The maximum texture intensity decreased down to 3.8 for the *D15TZ* axial region, which was as low as half the maximum texture intensity observed after swaging.

3.2. Electric resistivity measurement

The results of experimental measurement of electric resistivity of the CP Cu and both the *D15* and *D15TZ* conductors are summarized in **Figure 6**. The swaged conductors evidently featured higher conductivity than the commercially available Cu. This phenomenon can primarily be attributed to the differences in grain shapes. The grains within the original Cu were in the form of polyhedron, but elongated in the axial, i.e. swaging, direction after swaging (see the formation of texture fibres in **Figures 2b, 3b, 4b, and 5b**). The grain boundaries are among the main obstacles for moving electrons [3,6]. Therefore, the movement of electrons was aggravated within the original Cu featuring many obstacles due to the presence of numerous grain boundaries (polyhedrons) when compared to the *D15* swaged conductor featuring pancake-like grains elongated in the axial direction, i.e. the main direction of electrons movement. In other words, the elongated grains within the *D15* conductor enabled easier movement of electrons than their polyhedral counterparts within the CP Cu. The even increased conductivity observed for the *D15TZ* conductor was caused by decreased dislocation density within the grains' interiors. Due to the occurring softening processes (recovery/recrystallization), significant volume of dislocations annihilated or migrated to grain boundaries, by the effect of which the volume of "free space" for electrons movement increased. This was also related to the fact that the applied heat treatment reduced the developed substructure, i.e. supported the formation of full grains defined with HAGBs (compare the decrease in LAGBs portions in **Figures 2a** and **4a**, and **Figures 3a** and **5a**).

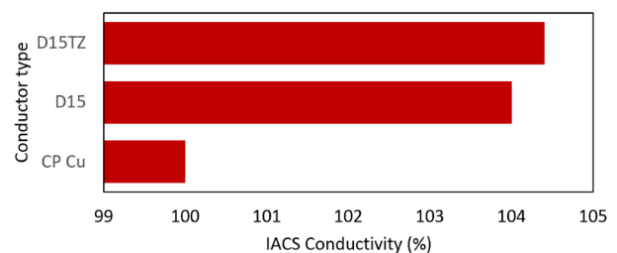


Figure 6 Comparison of electric conductivities for *D15* and *D15TZ* swaged conductors and CP Cu

4. CONCLUSIONS

The presented research assessed the effects of selected thermomechanical processing performed via room temperature rotary swaging and subsequent heat treatment on Cu conductors. It namely focused on correlation of microstructures and electric conductivity. Rotary swaging to the diameter of 15 mm imparted grain refinement and formation of texture fibres, i.e. the polyhedron-shaped randomly oriented large grains observed within the original Cu were transformed into refined and arranged pancake-like shaped grains by the swaging. This change in the grains' morphology was the main factor imparting the increase in electric conductivity to 104% IACS (100% IACS was measured for the commercially available original Cu). The conductivity of the 15 mm swaged and heat treated conductor then increased to 104.4% IACS as the applied annealing reduced the volume of dislocations and promoted transformation of substructure to full grains defined with high angle grain boundaries. The swaged and annealed conductor featured not only high volume fraction high angle grain boundaries (97%), but also almost 60% of $\langle 111 \rangle 60^\circ$ twin boundaries.

ACKNOWLEDGEMENTS

The research was supported by project no. 22-11949S by Czech Science Foundation.

REFERENCES

- [1] ZHILYAEV, A.P., SHAKHOVA, I., BELYAKOV, A., KAIBYSHEV, R., LANGDON, T.G. Effect of annealing on wear resistance and electroconductivity of copper processed by high-pressure torsion. *Journal of Materials Science*. 2014, vol. 49, pp. 2270–2278.
- [2] JIA, F., ZHAO, J., LUO, L., XIE, H., JIANG, Z. Experimental and numerical study on micro deep drawing with aluminium-copper composite material. *Procedia Engineering*. 2017, vol. 207, pp. 1051–1056.
- [3] RUSSELL, A., LEE, K.L. *Structure-Property Relations in Nonferrous Metals*. New Jersey, John Wiley & Sons Inc., 2005.
- [4] GENG, Y., BAN, Y., WANG, B., LI, X., SONG, K., ZHANG, Y., JIA, Y., TIAN, B., LIU, Y., VOLINSKY, A.A. A review of microstructure and texture evolution with nanoscale precipitates for copper alloys. *Journal of Materials Research and Technology*. 2020, vol. 9, pp. 11918–11934.
- [5] BABAHEYDARI, R.M., MIRABOOTALEBI, S.O., FAKHRABADI, G.H.A. Effect of Alloying Elements on Hardness and Electrical Conductivity of Cu Nanocomposites Prepared by Mechanical Alloying. *Iranian Journal of Materials Science and Engineering*. 2021, vol. 18, pp. 1–11.
- [6] KUNČICKÁ, L., KOCICH, R. Optimizing electric conductivity of innovative Al-Cu laminated composites via thermomechanical treatment. *Materials and Design*. 2022, vol. 215, 110441.
- [7] SUVOROVA, A.A., DANILOV, I. V., KALININ, G.M., KOROSTELEV, A.B. Heat treatment effects on the microstructure and properties of Cu–Cr–Zr alloy used for the ITER blanket components. *Nuclear Materials and Energy*. 2018, vol. 15 pp. 80–84.
- [8] KOCICH, R., LUKÁČ, P. SPD Processes - Methods for Mechanical Nanostructuring in: *Handbook of Mechanical Nanostructuring*. Weinheim: Wiley-VCH Verlag GmbH & Co. 2015: pp. 235–262.
- [9] KUNČICKÁ, L., KOCICH, R., LOWE, T.C. Advances in metals and alloys for joint replacement. *Progress in Materials Science*. 2017, vol. 88, pp. 232–280.
- [10] TIAN, Y.Z., FREUDENBERGER, J., PIPPAN, R., ZHANG, Z.F. Formation of nanostructure and abnormal annealing behavior of a Cu-Ag-Zr alloy processed by high-pressure torsion. *Materials Science and Engineering A*. 2013, vol. 568, pp. 184–194.
- [11] HLAVÁČ, L.M., KOCICH, R., GEMBALOVÁ, L., JONŠTA, P., HLAVÁČOVÁ, I.M. AWJ cutting of copper processed by ECAP. *International Journal of Advanced Manufacturing Technology*. 2016, vol. 86, pp. 885–894.
- [12] KOCICH, R., FIALA, J., SZURMAN, I., MACHÁČKOVÁ, A., MIHOLA, M. TWIST-channel angular pressing: effect of the strain path on grain refinement and mechanical properties of copper. *Journal of Materials Science*. 2011, vol. 46, pp. 7865–7876.
- [13] KOCICH, R., MACHÁČKOVÁ, A., KUNČICKÁ, L. Twist channel multi-angular pressing (TCMAP) as a new SPD process: Numerical and experimental study. *Materials Science and Engineering A*. 2014, vol. 612, pp. 445–455.
- [14] NOSRATI, H.G., KHALILI, K., GERDOOEI, M. Theoretical and experimental evaluation of no-slip feeding condition in ECAP-Conform of a square-section metallic rod. *The International Journal of Advanced Manufacturing Technology*. 2021, vol. 112, pp. 375–385.
- [15] BAHADORI, S.R., DEGHANI, K., AKBARI MOUSAVI, S.A.A. Comparison of microstructure and mechanical properties of pure copper processed by twist extrusion and equal channel angular pressing. *Materials Letters*. 2015, vol. 152, pp. 48–52.
- [16] JAMILI, A.M., ZAREI-HANZAKI, A., ABEDI, H.R., MOSAYEBI, M., KOCICH, R., KUNČICKÁ, L. Development of fresh and fully recrystallized microstructures through friction stir processing of a rare earth bearing magnesium alloy. *Materials Science and Engineering A*. 2019, vol. 775, pp. 138837.
- [17] KOCICH, R., MACHÁČKOVÁ, A., FOJTÍK, F. Comparison of strain and stress conditions in conventional and ARB rolling processes. *International Journal of Mechanical Sciences*. 2012, vol. 64, pp. 54–61.
- [18] STRUNZ, P., KOCICH, R., CANELO-YUBERO, D., MACHÁČKOVÁ, A., BERAN, P., KRÁTKÁ, L. Texture and Differential Stress Development in W/Ni-Co Composite after Rotary Swaging. *Materials*. 2020, vol. 13, 2869.
- [19] KOCICH, R. Design and optimization of induction heating for tungsten heavy alloy prior to rotary swaging, *International Journal of Refractory Metals and Hard Materials*. 2020, vol. 93, 105353.
- [20] VERLINDEN, B., DRIVER, J., SAMAJDAR, I., DOHERTY, R.D. *Thermo-mechanical processing of metallic materials*. Amsterdam: Elsevier, 2007.